Welding Seam Image Dust Removal Algorithm Based on Fusion of Dual-scale Dark Channel and Bright Channel

Qingchun Zheng, Zhidong Zhang, Jingna Liu*, Peihao Zhu, and Wenpeng Ma

Abstract—**The dust removal technology of welding seam image has important practical significance for promoting the development of weld instance segmentation and target tracking. In this paper, we propose a welding seam image dust removal algorithm based on fusion of dual-scale dark channel and bright channel, which is to solve the problem that the color distortion and halo effect of dark channel prior image restoration algorithm in weld depth of field sudden change area and bright region. Firstly, the results of the minimum filtering of two scale windows are adaptively weighted and fused to obtain the fused dark channel. Secondly, the dark channel prior and the bright channel prior fusion strategy is adopted to obtain the fused atmospheric light to make the rough transmittance estimation more accurate. Finally, the weighted guided filtering is combined with up-sampling and down-sampling to optimize the rough transmittance, and the weld image is restored by combining the atmospheric scattering model. The experimental results indicate that our algorithm can restore the color and edge details of welding seam images and effectively suppress the halo effect. The objective comparison with several typical algorithms proves the feasibility and superiority of the proposed algorithm.**

Index Terms—**image restoration, dedusting, dark channel prior, bright channel, weighted guided filtering.**

I. Introduction

WITH the rapid development of intelligent manufacturing, efficient and accurate welding seam detection, segmentation, and target tracking technologies are required for welding seam grinding and polishing automation. However, there is often a large amount of dust in the welding seam grinding and polishing workshop, and the interaction between dust particles and the reflected light of smooth welding seam makes it difficult for the indoor welding seam image acquisition system to obtain clear images of welding seam without noise interference, which seriously affects the accuracy of welding seam detection and efficiency of welding seam grinding and polishing [1]. Therefore, dust removal processing on weld images collected in dusty environment has important value for the automation of complex weld grinding.

Manuscript received September 20, 2020; revised February 14, 2021. This work was supported by the National Natural Science Foundation of China (Grant No.62073239 and 61941305) and the Natural Science Foundation of Tianjin, China (Grant No.18JCQNJC75000).

Qingchun Zheng is a Professor in the Key Laboratory of Advanced Mechatronic System Design and Intelligent Control, Tianjin University of Technology, Tianjin 300384, China. (e-mail: zhengqingchun@tjut.edu.cn).

Zhidong Zhang is a postgraduate student in the Key Laboratory of Advanced Mechatronic System Design and Intelligent Control, Tianjin University of Technology, Tianjin 300384, China. (e-mail: 978608658@qq.com).

Jingna Liu is a Lecturer in the Key Laboratory of Advanced Mechatronic System Design and Intelligent Control, Tianjin University of Technology, Tianjin 300384, China. (corresponding author, phone: (+86)13821826079; e-mail: liujingna2003@163.com).

Peihao Zhu is an Assistant Professor in the Key Laboratory of Advanced Mechatronic System Design and Intelligent Control, Tianjin University of Technology, Tianjin 300384, China. (e-mail:zhupeihao_gp@163.com).

Wenpeng Ma is a Lecturer in the Key Laboratory of Advanced Mechatronic System Design and Intelligent Control, Tianjin University of Technology, Tianjin 300384, China. (e-mail: wenpengma@sina.com).

Currently, there are two mainstream methods to make the image of welds containing dust clear: one is based on the image enhancement method, which mainly includes a series of algorithms derived from the Retinex algorithm [2], histogram equalization [3], [4], wavelet transform [5], bilateral filtering [6] and so on. This method can improve the contrast of the image to improve the image quality without considering the essential reasons of image degradation, but the introduction of corresponding noise will easily lead to incomplete details of the restored image, resulting in edge blurring and distortion. The other is based on the physical model method, which analyzes physical process of image degradation, and uses priori or hypothesis to clear the weld image in the inverse process of image degradation. This method is widely used because it is not affected by the external environment.

In recent years, using many assumptions and prior knowledge, single image restoration has made considerable progress. Fattal [7] estimated the reflectivity of scene and achieved image restoration by using the independent component analysis method, which is based on the priori that the reflectivity of object surface is not correlated with the local statistics of transmission value. However, the algorithm requires image to have bright color, and the restoration effect is not ideal for the image without enough color prior information. Tarel [8] used median filtering to estimate atmospheric dissipation function to restore image. This method can restore the image quickly, but the extracted depth map fails to keep edge details well, so that the processing effect is not ideal in areas with sudden changes in depth of field and highlighted areas. He [9] found and proposed dark channel prior theory, the use of prior knowledge to estimate the transmittance, and with the atmospheric scattering model for the successful implementation of image restoration. Considering that the visible detail blurring and halo effect of the restored image, the rough transmission was optimized by soft-matting algorithm [10] which was time-consuming in calculation. He [11] also proposed to use guided filtering to obtain a better restoration effect. Since then, researchers have successively proposed the dark channel prior algorithm combining the mixed bilateral filtering [12] and mean filtering [13], as well as the multi-scale Retinex algorithm [14] to improve the effectiveness of the algorithm. However, the processing effect of these algorithms in the image highlights and edge areas is poor, and it is easy to produce halo effect or serious color distortion.

To sum up, the previous research work provides different ideas for the dust removal of welding seam images. In this paper, we fuse the dual-scale dark channel and the bright channel for dedusting, which improves the traditional dark channel prior method. Firstly, considering that the dark channel prior expected effects on the minimum filtering of different window scales are inconsistent, so the fused dark channel is obtained by approximating the depth of field relationship and adaptively weighting the results of the two scale templates. Secondly, considering the correlation between atmospheric light and transmittance, the prior fusion strategy of dark channel and bright channel is used for obtaining the fused atmospheric light to make the rough transmittance estimation more accurate. Finally, the fast-weighted guided filter combined with the variance information in the local window is used to refine the rough transmittance, so as to improve the dust removal effect of the weld edge area and flat area in the image. Experimental results indicate that our algorithm can restore the color and edge details of weld images and effectively suppress halo effect.

II. Dark Channel Priori Theory

In the field of image processing and computer vision, the atmospheric scattering model [15] for image restoration is expressed as:

$$I(x) = J(x)t(x) + A[1 - t(x)] \tag{1}$$

where $I(x)$ is original image, $J(x)$ is restored image, $t(x)$ is transmittance which describes the portion of light intensity reaching the imaging device after medium transmission, A is atmospheric light value, x represents the spatial position of a pixel in the image. On the right side of (1), the first term $J(x)t(x)$ is direct attenuation, and the second term $A[1 - t(x)]$ is atmospheric dissipation function which causes the scene color of the image to shift.

The goal of image restoration is to recover $J(x)$ according to $I(x)$, $t(x)$, and A. However, it is clear that (1) has multiple solutions, so a strong hypothesis or a priori is required to accurately restore a clear image.

Based on the atmospheric scattering model, He [9] obtained a priori knowledge of the dark channel through observation and statistics of many outdoor fog-free images, that is, most of the non-sky patches in images contain some pixels whose intensity value is very low or close to zero, and for any clear image, the dark channel can be calculated as the minimum value of all pixels in a local area. Generally, the dark channel J^{dark} can be expressed as:

$$J^{dark}(x) = \min_{c\in\{r,g,b\}}\left(\min_{y\in\Omega(x)}(J^c(y))\right) \approx 0 \tag{2}$$

where $J^c(y)$ is the three color channels of $J(x)$, $\Omega(x)$ represents a square filtering window with radius x as the center, and is usually set as 15×15.

In the case that A is known, divide A both sides of (1) at the same time to obtain:

$$\frac{I^c(x)}{A^c} = t(x)\frac{J^c(x)}{A^c} + 1 - t(x) \tag{3}$$

Assuming that the transmission value is constant in the neighborhood of $\Omega(x)$, denote it as $\tilde{t}(x)$, and the minimum value of both sides of (3) is calculated at the same time.

$$\min_{y\in\Omega(x)}(\min_{c\in\{r,g,b\}}\frac{I^c(y)}{A^c}) = \tilde{t}(x)\min_{y\in\Omega(x)}(\min_{c\in\{r,g,b\}}\frac{J^c(y)}{A^c}) + 1 - t(x) \tag{4}$$

Combined with (4) and (2), the transmittance can be obtained as follows:

$$t(x) = 1 - \omega\min_{y\in\Omega(x)}(\min_{c\in\{r,g,b\}}\frac{I^c(y)}{A^c}) \tag{5}$$

where $t(x)$ is rough transmittance. In order to make the restored image close to the real scene reflection, an adjustment coefficient ω is introduced, and its value is usually set 0.95.

Given the values of parameters $t(x)$ and A, the restored welding seam image $J(x)$ can be expressed as:

$$J(x) = \frac{I(x) + A}{\max(t(x), t_0)} + A \tag{6}$$

where t_0 is a protection factor to prevent the distortion of restored image due to $t(x)$ too small, and it is best to take as 0.1.

III. Proposed Algorithm

In the process of acquiring the dark channel by the traditional dark channel prior algorithm, the minimum filtering of single scale window can obtain the dark channel value with high accuracy, while the fineness of the corresponding transmission image decreases, resulting in obvious blocky effect in the restored image. In addition, due to the large area of bright white weld, the atmospheric light value predicted by the dark channel prior algorithm will be inaccurate, resulting in color distortion and blurred weld edge details in the final restored image. Since dark channel prior is prone to halo effect and color distortion in weld depth of field sudden change area and bright region, a new algorithm based on

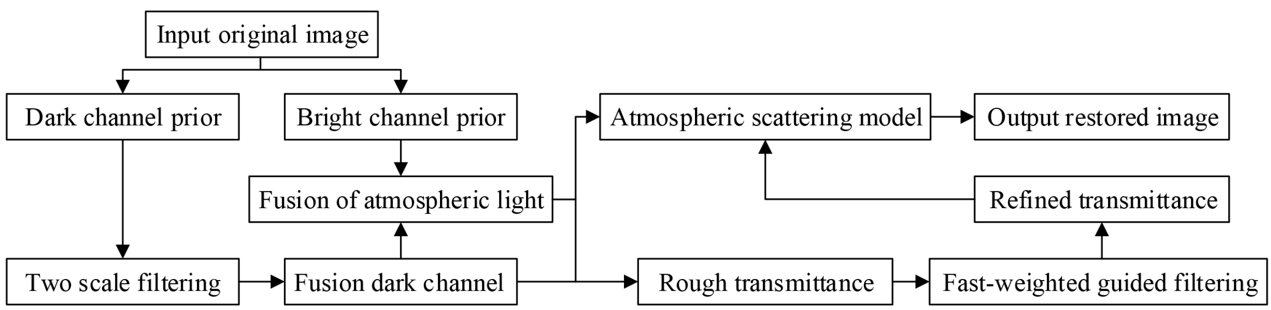

Fig. 1. Flowchart of the proposed method.

fusion of dual-scale dark channel and bright channel is proposed. The algorithm flowchart is shown in Fig. 1.

A. Fusion of Dark Channel

In the process of obtaining the dark channel, the R, G, and B three channels of the pixels in the image sliding window are subjected to minimum filtering according to the dark channel prior. With the gradual increase of the minimum filter window scale, the number of pixels participating in the same sliding window will gradually increase. Meanwhile, there are fewer and fewer gray levels in the dark channel map but more and more image areas with lower gray values, which causes the accuracy of the dark channel value obtained is higher. However, when the dark channel value is used to calculate the transmittance, the assumption that the transmittance in the same sliding window is regarded as a fixed value will become inaccurate with the increase of the window size. The fineness of the transmittance image gradually decreases, and the halo effect in the restored image is more and more obvious.

For the same original weld image (Fig. 2a), Fig. 2b–2d shows the obtained transmittance map is relatively fine, and the restored image will not have too much distortion and obvious halo effect when the minimum filter window scale is 5×5. However, due to the inaccuracy of the corresponding dark channel value, the restored weld image is supersaturated. By contrast, as shown in Fig. 2e–2g, when the minimum filter window scale is 15×15, the accurate dark channel value can be obtained, but the fineness of the corresponding transmittance map decreases, resulting in obvious halo effect in the restored weld image.

Considering that the dark channel prior expected effects of the minimum filtering of different window scales are inconsistent, this paper proposes a method of combining dark channel priors to avoid the halo effect in the sudden change of image depth regions. The dark channels of large-scale window filter and small-scale window filter are calculated respectively, and the fused dark channel is obtained by adaptive weighted fusion of the two minimum filtering results through approximate depth of field relationship, a weighted fusion is determined by:

$$I^{dark}(x) = a_1 I_1^{dark}(x) + a_2 I_2^{dark}(x) \tag{7}$$

where $I^{dark}(x)$ is the fusion dark channel of original image, $I_1^{dark}(x)$ is the dark channel obtained by minimum filtering of window scale 5×5, and $I_2^{dark}(x)$ is the dark channel obtained by minimum filtering of window scale 15×15, a_1 and a_2 are weighted fusion coefficients that satisfy the condition $a_1 + a_2 = 1$.

The relationship between depth of field information and brightness and saturation is proposed in [16]. The depth of field information is approximately estimated by the brightness and saturation of the image, and the weighted fusion coefficient $a_2(x)$ is defined by:

$$V_s(x) = \min_{\Omega(x)}[V(x) - S(x)] \tag{8}$$

$$a_2(x) = e^{-\frac{(\mu - V_s(x))^2}{2\sigma^2}} \tag{9}$$

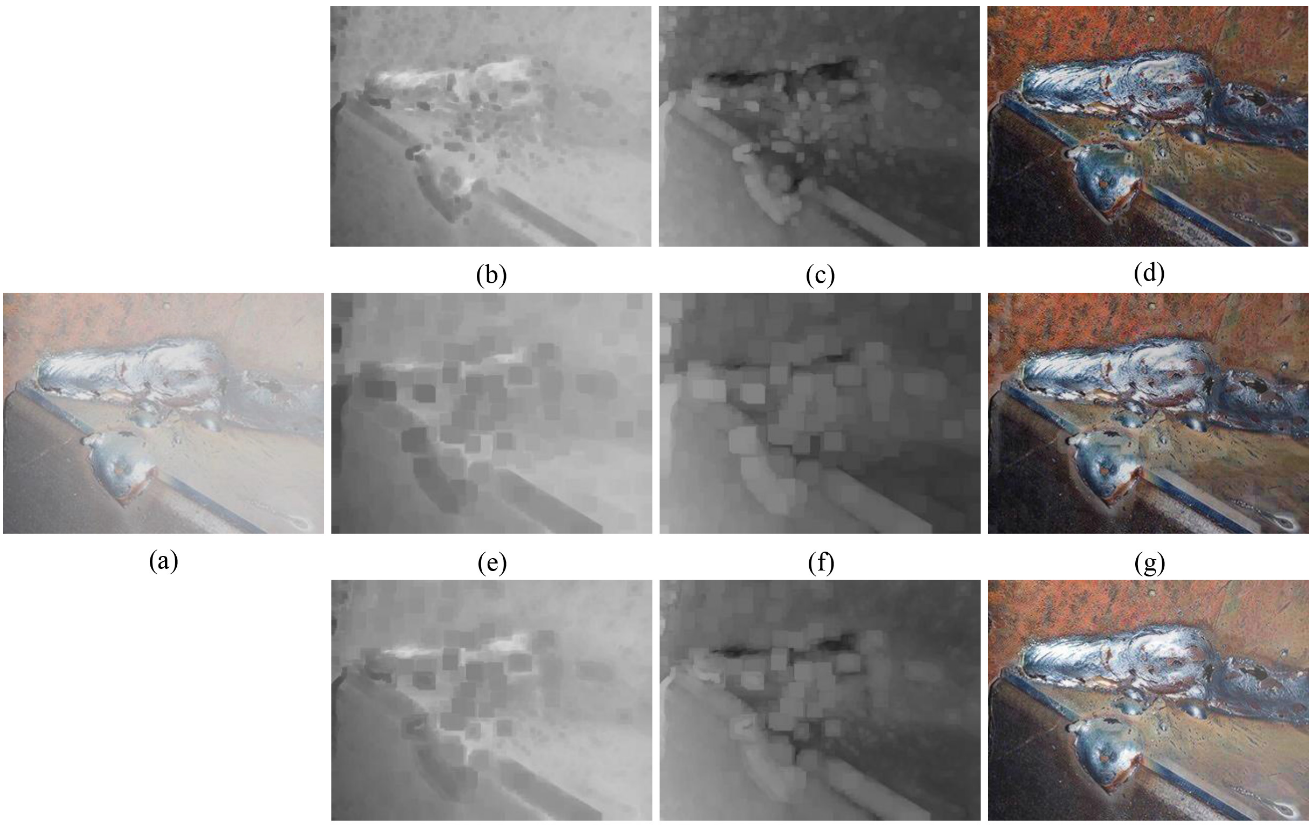

(a) (b) (c) (d) (e) (f) (g) (h) (i) (j)

Fig. 2. Dark channel comparison. (a) Original weld image, (b) Dark channel (5×5), (c) Transmittance (5×5), (d) Result using (b) (5×5), (e) Dark channel (15×15), (f) Transmittance (15×15), (g) Result using (e) (15×15), (h) Fusion dark channel, (i) Corresponding transmittance, (j) Result using (h).

In (8), $V_s(x)$ is approximate depth of field, $V(x)$ is brightness component of original image, $S(x)$ is saturation component of original image, and $\Omega(x)$ is minimum filtering of window scale 15×15. In (9), $a_2(x)$ is Gaussian weight coefficient, μ is expected value, and σ is standard deviation, and the effect is best when both are taken as 0.5.

As shown in Fig. 2h–2j, the fusion dark channel can effectively reduce the halo effect in the restored image and obtain a higher accuracy of the dark channel value.

B. Atmospheric Light Value Estimation

Atmospheric light value A is an important parameter of image restoration algorithm based on atmospheric scattering model, and its accuracy directly determines the quality of restored image. In the dark channel prior, the first 0.1% brightest pixel in the dark channel map is used, and the corresponding maximum pixel value in the original image is selected as atmospheric light value A [9].

However, due to the large area of bright white weld in the image, A will be inaccurate, resulting in color distortion and blurred weld edge details in the final restored image. To solve this problem, a prior fusion strategy of dark channel and bright channel is proposed to obtain the fused atmospheric light value.

Yan's theory of bright channel is similar to the prior of dark channel [17]. Its basic idea is that in most blurred images, some pixels always have at least one color channel with greater intensity, and even the intensity value is close to 255, so the bright channel can be expressed by

$$J^{bright}(x) = \max_{y\in\Omega(x)}[\max_{c\in\{r,g,b\}} J^c(y)] \to 255 \tag{10}$$

In order to illustrate the difference between the dark channel and the bright channel, several original images, dark channel maps and bright channel maps are given, which is shown in Fig. 3. Among them, Fig. 3a is the original weld image, Fig. 3b is the corresponding fusion dark channel, and Fig. 3c is the corresponding bright channel.

As shown in Fig. 3c, the intensity value of bright channel tends to the atmospheric light intensity of clear image according to the prior theory of bright channel, which can be expressed by

$$A^{light}(x) = \max_{c\in\{r,g,b\}}[\max_{y\in\Omega(x)} I^c(y)] \tag{11}$$

The atmospheric light value is estimated by introducing fusion dark channel and bright channel regulators, and the final fused atmospheric light $A(x)$ is defined by:

$$A(x) = \alpha A^{light}(x) + \beta A_0 \tag{12}$$

where $A^{light}(x)$ is the atmospheric light estimation of the bright channel, A_0 is the mean value of pixels in the corresponding position of original image of the first 0.1% maximum pixel in the fusion dark channel, α and β are fusion coefficients that satisfy the condition $\alpha+\beta < 1.0$, and the effect is best when $\alpha = 0.5$ and $\beta = 0.45$.

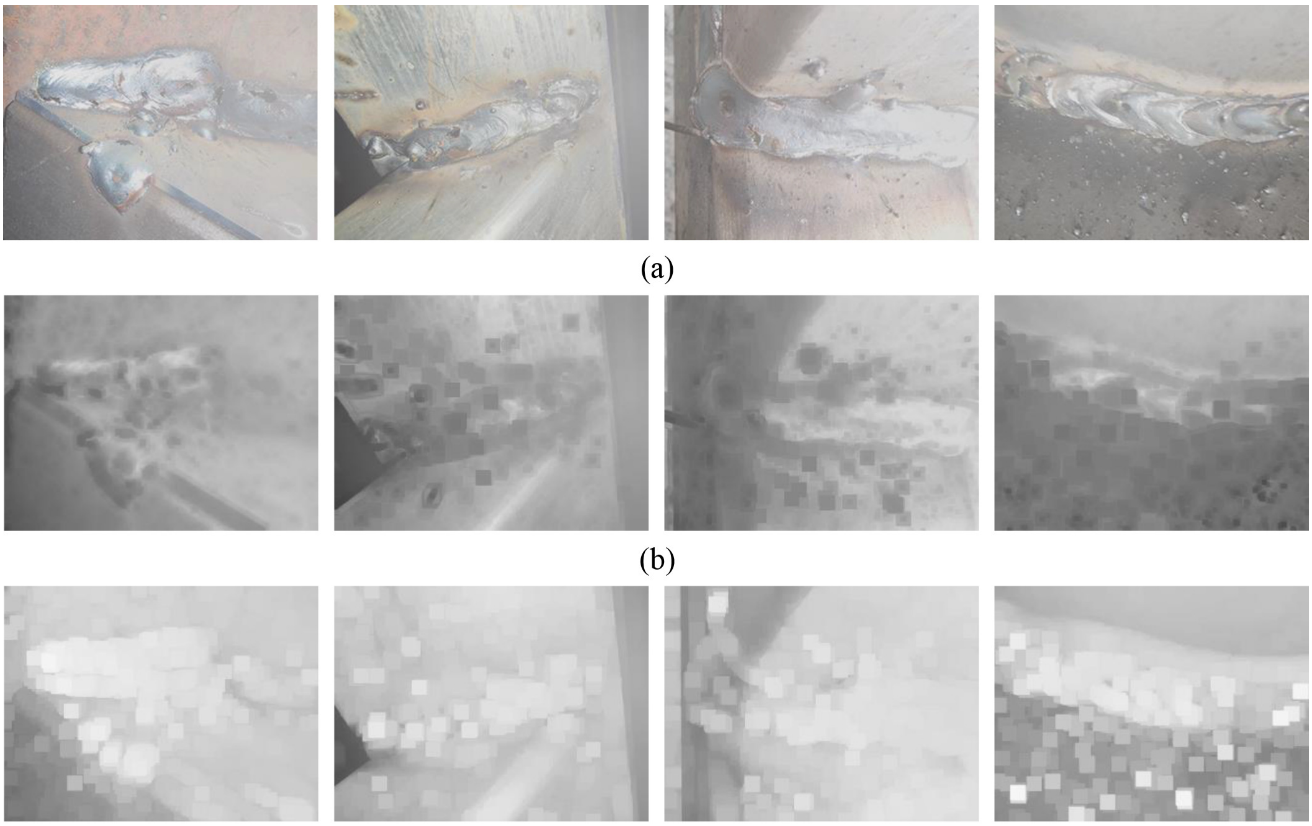

(a)

(b)

(c)

Fig. 3. Fusion dark channel images and bright channal images. (a) Original image, (b) Fusion dark channel, (c) Bright channal.

C. Optimized Transmission

Because the restored image is still a little halo effect via minimum filtering operation, and it can be seen from Fig. 2j that some parts are unnaturally restored. To further remove halo effect and refine contour, the fast-weighted guided filtering combined with up-sampling and down-sampling is used to optimize the rough transmittance. The input guide image of weighted guided filtering is defined as I, the image before filtering is p, and the image after filtering is q. q and I satisfy the local linear relationship in the window ω_k centered at pixel point k.

$$q_i = a_k I_i + b_k, \forall i \in \omega_k \tag{13}$$

where a_k and b_k are fixed coefficients, which should satisfy the condition that the difference between p and q is minimized, so the loss function model $E(a_k, b_k)$ is defined by:

$$E(a_k, b_k) = \sum_{i \in \omega_k} \left[(a_k I_i + b_k - p_i)^2 + \varepsilon a_k^2 \right] \tag{14}$$

where ε is a punishment parameter to prevent a_k from being too large, and in order to adjust the regularization factor adaptively by combining the variance information in ω_k, the edge perception weight $\Gamma_I(i)$ is expressed by:

$$\Gamma_I(i) = \frac{1}{N} \sum_{i'=1}^{N} \frac{\sigma_I^2(i) + \gamma_\sigma}{\sigma_I^2(i') + \gamma_\sigma} \tag{15}$$

where γ_σ is a small constant whose value is $(0.001 \times L)^2$, L is the range of gray value, and N is the total number of pixels in I.

Combined with (14) and (15), the new loss function model $E(a_k, b_k)$ is defined by:

$$E(a_k, b_k) = \sum_{i \in \omega_k} \left[(a_k I_i + b_k - p_i)^2 + \frac{\varepsilon}{\Gamma_I(i)} a_k^2 \right] \tag{16}$$

$$a_k = \frac{\frac{1}{|\omega|} \sum_{i \in \omega_k} I_i p_i - \mu_k \bar{p}_k}{\sigma_k^2 + \frac{\varepsilon}{\Gamma_I(i)}} \tag{17}$$

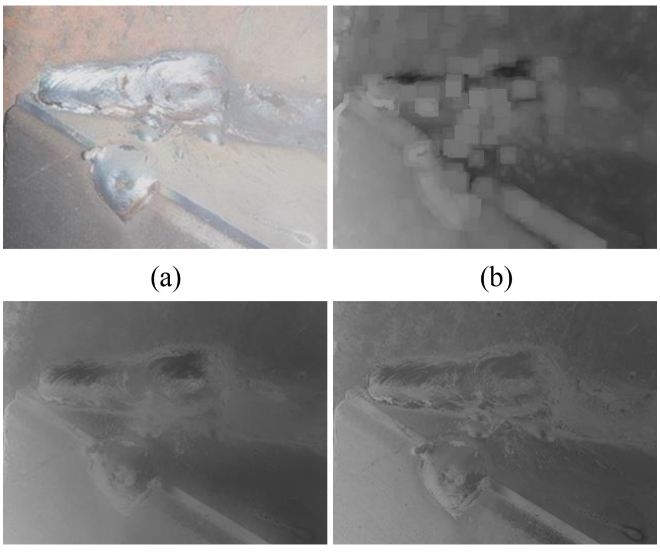

(a) (b)

(c) (d)

Fig. 4. Transmission optimization results. (a) Original weld image, (b) Rough transmission, (c) Guided filtering [11], (d) Fast-weighted guided filtering.

$$b_k = \bar{p}_k - a_k \mu_k \tag{18}$$

where μ_k and σ_k^2 are the mean and variable of I in ω_k, $|\omega|$ is the number of pixels in ω_k, and $\bar{p}_k$ is the mean of p in ω_k. Finally, the filtered output is determined by:

$$q_i = \bar{a}_i I_i + \bar{b}_i \tag{19}$$

where $\bar{a}_i$ and $\bar{b}_i$ represent the mean values of a_i and b_i in ω_k, respectively.

In this research, the original weld image is taken as I (Fig. 4a), the rough transmittance is taken as p (Fig. 4b), and the refined transmittance is taken as q. I' and p' are obtained by down-sampling I and p, the linear coefficients a, b of the guided filtering are calculated by I' and p', and q is up-sampled by bilinear interpolation. By combining the weight of edge perception to reduce noise, and assigning a larger weight in the depth discontinuity area, the fast-weighted guided filtering can improve the dust removal effect of the weld edge area and flat area in the image. As given in Fig. 4d, compared with [11] (Fig. 4c), its effect in maintaining the edge information of weld image is better.

IV. Experiment Results and Analyses

In order to verify the restoration effect of our algorithm on the weld images, the experimental results are compared with the classical image restoration algorithm, and the dust removal effect is evaluated from both subjective and objective aspects. The experiment is implemented on MATLAB2018b, the processor is Intel (R) Xeon (R) Gold 5118 CPU @ 2.30GHz, and the running environment is Windows10.

A. Subjective Evaluation

Subjective evaluation can directly and quickly distinguish the advantages and disadvantages of the restored image. In this paper, four classical image restoration algorithms are selected to compare with the proposed algorithm. Fig. 5 shows the comparison of dedusting effects of different algorithms. Among them, Fig. 5a is the original weld image with poor visibility. Fig. 5b shows the dust removal effect of image restoration algorithm proposed in [7], which uses independent component analysis to estimate the reflectivity of the scene. The color saturation of the bright white area of the restored weld image is too high, which leads to the blurring of the weld edge details. Fig. 5c shows the results of image restoration algorithm proposed in [8], which uses median filtering to estimate the atmospheric dissipation function. The overall color of the processed image can be maintained, but the effect of dust removal is not obvious. Fig. 5d shows the dust removal effect of dark channel prior algorithm [11]. Although the dust at weld edge was effectively removed, the overall restoration image is darkened and contour is blurred due to the inaccurate atmospheric light estimation. In addition, obvious color darkening and halo effect appear in the bright area of weld. Fig. 5e shows the dedusting effect of multi-scale Retinex based on image enhancement [14]. There is no halo effect in restored image, and the visibility is better, but this method causes local contrast reduction and severe color misalignment. Fig. 5f shows the dust removal effect of algorithm we proposed. Compared with the above four algorithms, the restored image has rich details and clear

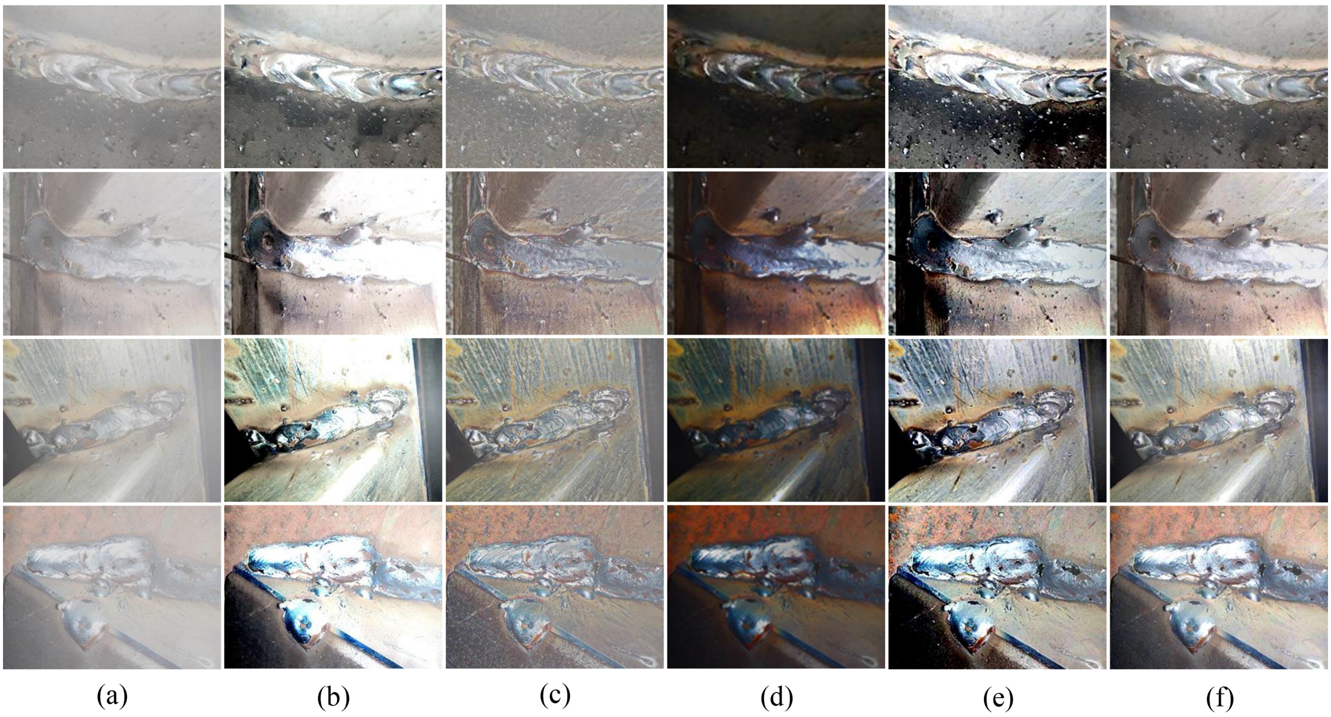

Fig. 5. Contrast of weld image restoration effect. (a) Original images, (b) Fattal's result [7], (c) Tarel's result [8], (d) He's result [11], (e) Zhao's result [14], (f) Our result.

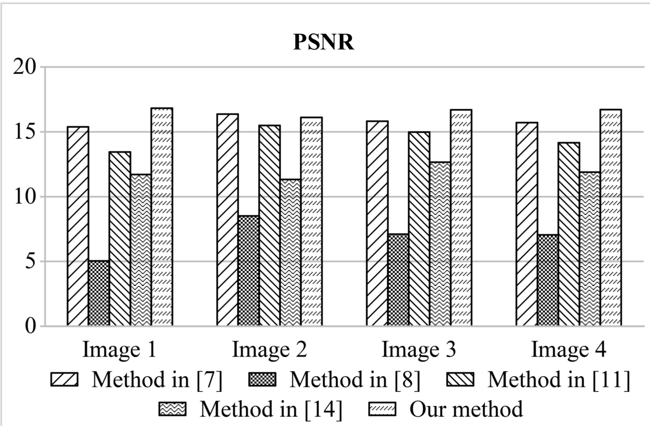

Fig. 6. Graph of peak signal-to-noise ratio of image processed by different restoration algorithms.

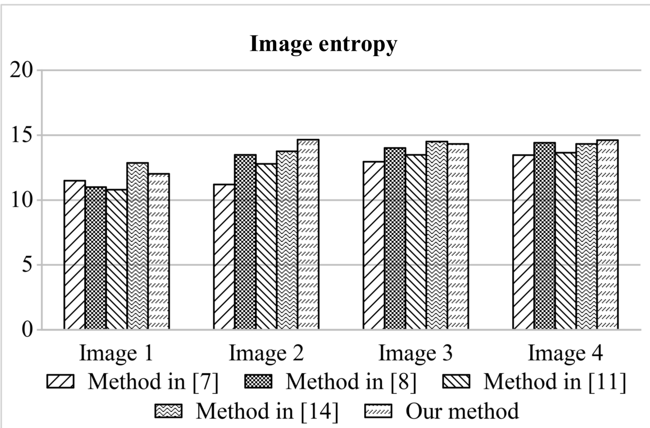

Fig. 7. Graph of entropy measurement of image processed by different restoration algorithms.

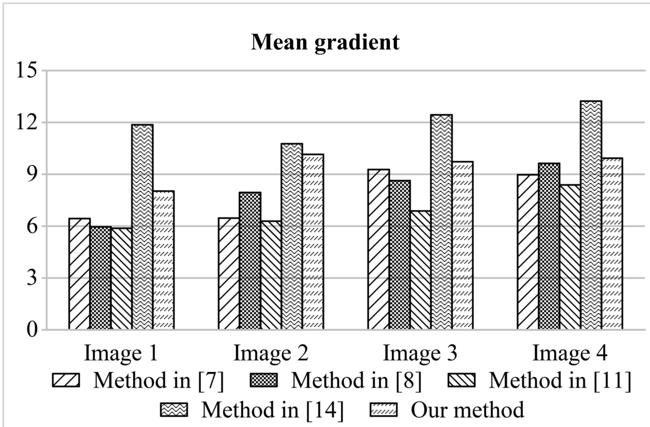

Fig. 8. Graph of mean gradient of image processed by different restoration algorithms.

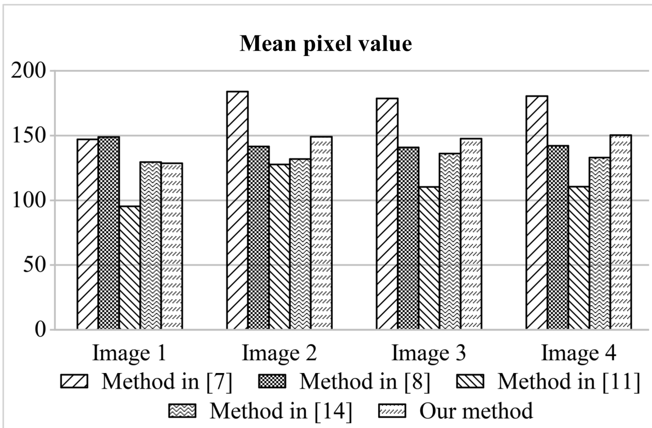

Fig. 9. Graph of mean pixel value of image processed by different restoration algorithms.

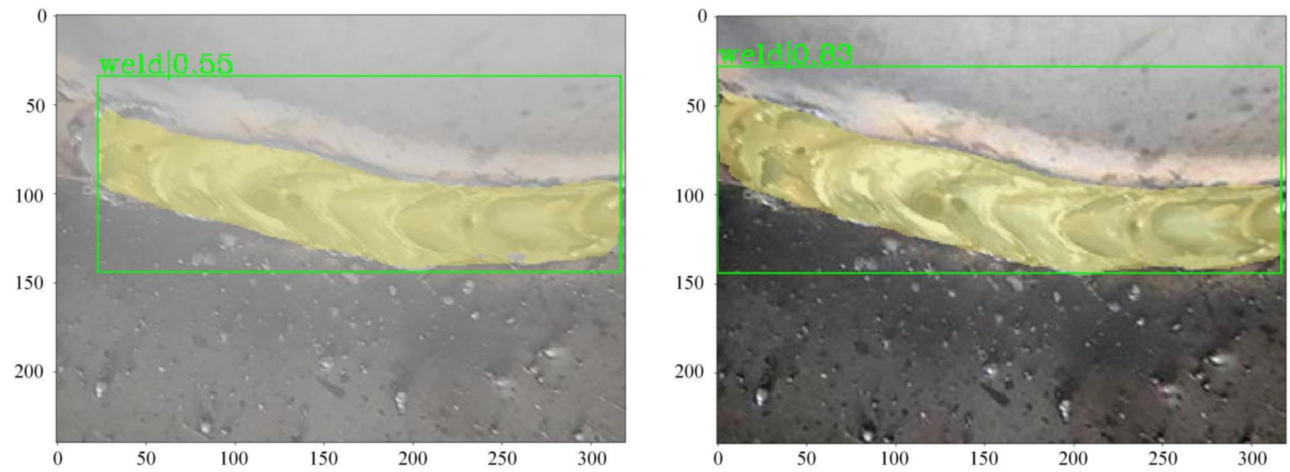

(a) (b)

Fig. 10. Weld instance segmentation. (a) Original image, (b) Restored image.

weld contour due to the introduction of bright channel to compensate brightness and contrast without obvious color distortion and halo effect.

B. Objective Evaluation

Although the subjective evaluation is direct and effective, the difference of subjects may lead to different subjective evaluation. In order to further verify the objective effectiveness of method we proposed, the peak signal-to-noise ratio (PSNR), color image entropy, mean gradient of image, and mean pixel value are used as evaluation indexes in this paper [18], [19], [20], [21]. It can be seen from Fig. 6 that the proposed algorithm has achieved good dust removal effect compared with the classical algorithm. Among them, the method proposed in [8] has a low index because the effect of dust removal is not obvious. Fig. 7 shows that the algorithm we proposed can effectively eliminate the halo effect and maintain the detailed information in the restored image. Fig. 8 shows that the algorithm we proposed and [14] are better than other methods in terms of weld edge transition effect. It can be seen from Fig. 9 that the overall image restored by the traditional dark channel prior is dark, which leads to the low average pixel value of the image, and the introduction of bright channel in proposed algorithm can effectively compensate for the brightness loss.

C. Weld Instance Segmentation

In order to verify the practicability of the images processed by the proposed algorithm, 100 original images with dust and 100 corresponding restored images are taken as training datasets of Mask RCNN segmentation framework to transfer learning based on the deep learning target detection toolbox MMDetection [22], [23]. Finally, the trained model is used to segment the original image and restored image respectively. The experimental platform is built in the Windows system, and the graphics card is RTX2080Ti. As shown in Fig. 10, the weld boundary of the original image is not completely segmented (Fig. 10a), the segmentation of the restored image weld is more delicate, and the confidence score of the weld detection has been greatly improved (Fig. 10b). Therefore, the restored images as a dataset is helpful to improve the effect of weld target detection and instance segmentation.

V. Conclusion

According to the research of dust removal by using prior algorithm of dark channel, and aiming to solve the problems of color distortion and halo effect of restored image, a new algorithm based on fusion of dual-scale dark channel and bright channel is proposed in this paper. In order to obtain high accuracy dark channel values and correct the corresponding transmission region, the adaptive weighted fusion dark channel is derived by approximating the depth of field relationship. The bright channel prior is introduced to avoid the influence of large area bright white weld area and effectively compensate for the brightness loss. The experimental results indicate that our algorithm can effectively improve the weld edge details and suppress halo effect. Besides, the restored image has high contrast and strong visibility. However, there are still some shortcomings in the algorithm, which is the direction of follow-up research to adaptively fuse the dark channel and the bright channel to obtain a more accurate atmospheric light estimation and further improve the effect of removing dust from the weld image.

References

[1] R. Ranjan, A. R. Khan, C. Parikh, R. Jain, R. P. Mahto, et al, “Classification and identification of surface defects in friction stir welding: An image processing approach,” *Journal of Manufacturing Processes*, vol. 22, pp237-253, 2016.

[2] W. Wang, B. Li, J. Zheng, S. Xian, and J. Wang, “A fast Multi-Scale Retinex algorithm for color image enhancement,” in *IEEE International Conference on Wavelet Analysis and Pattern Recognition 2008*, 30-31 August, 2008, Hong Kong, China, pp80-85.

[3] M. Abdullah-Al-Wadud, M. H. Kabir, M. A. A. Dewan, and O. Chae, “A dynamic histogram equalization for image contrast enhancement,” in *Digest of Technical Papers International Conference on Consumer Electronics (ICCE) 2007*, 10-14 January, 2007, Las Vegas, U.S.A., pp593-600.

[4] S. Swee, L. Chen, and T. Ching, “Contrast enhancement in endoscopic images using fusion exposure histogram equalization,” *Engineering Letters*, vol. 28, no. 3, pp73-81, 2020.

[5] Y. Du, B. Guindon, and J. Cihlar, “Haze detection and removal in high resolution satellite image with wavelet analysis,” *IEEE Transactions on Geoence & Remote Sensing*, vol. 40, no. 1, pp210-217, 2002.

[6] H. Lu, Y. Li, L. Zhang, A. Yamawaki, S. Yang, et al, "Underwater optical image dehazing using guided trigonometric bilateral filtering," in *IEEE International Symposium on Circuits and Systems (ISCAS) 2013*, 19-23 May, 2013, Beijing, China, pp2147-2150.
[7] R. Fattal, "Single image dehazing," *Association for Computing Machinery Transactions on Graphics*, vol. 27, no. 3, pp1-9, 2008.
[8] J. P. Tarel and N. Hautière, "Fast visibility restoration from a single color or gray level image," in *IEEE 12th International Conference on Computer Vision (ICCV) 2009*, 29 September-2 October, 2009, Kyoto, Japan, pp2201-2208.
[9] K. He, J. Sun, and X. Tang, "Single image haze removal using dark channel prior," in *IEEE Computer Society Conference on Computer Vision and Pattern Recognition 2009*, 20-25 June, 2009, Miami, U.S.A., pp1956-1963.
[10] K. He, J. Sun, and X. Tang, "Single image haze removal using dark channel prior," *IEEE Transactions on Pattern Analysis & Machine Intelligence*, vol. 33, no. 12, pp2341-2353, 2011.
[11] K. He, J. Sun, and X. Tang, "Guided image filtering," *IEEE Transactions on Pattern Analysis & Machine Intelligence*, vol. 35, no. 6, pp1397-1409, 2013.
[12] A. K. Tripath and S. Mukhopadhyay, "Single image fog removal using bilateral filter," in *IEEE International Conference on Signal Processing, Computing and Control, ISPCC 2012*, 15-17 March, 2012, Waknaghat Solan, India, pp1-6.
[13] D. Meng and W. Li, "Single-image haze removal using the mean vector L2-norm of RGB image sample window," *Optik - International Journal for Light and Electron Optics*, vol. 126, no. 23, pp3522-3528, 2015.
[14] C. Zhao and J. Dong, "Image enhancement algorithm of haze weather based on dark channel and multi-scale Retinex," *Laser Journal*, vol. 39, no. 1, pp104-109, 2018.
[15] E. J. Mccartney and F. F. Hall, "Optics of the Atmosphere: Scattering by Molecules and Particles," *Physics Today*, vol. 30, no. 5, pp76-77, 1977.
[16] Q. Zhu, J. Mai, and L. Shao, "A fast single image haze removal algorithm using color attenuation prior", *IEEE Transactions on Image Processing*, vol. 24, no. 11, pp3522-3533, 2015.
[17] Y. Yan, W. Ren, Y. Guo, R. Wang, and X. Cao, "Image deblurring via extreme channels prior," in *30th IEEE Conference on Computer Vision and Pattern Recognition (CVPR) 2017*, 21-26 July, 2017, Honolulu, U.S.A., pp6978-6986.
[18] J. Zhang, X. Wang, C. Yang, J. Zhang, D. He, et al, "Image dehazing based on dark channel prior and brightness enhancement for agricultural remote sensing images from consumer-grade cameras," *Computers and Electronics in Agriculture*, vol. 151, pp196-206, 2018.
[19] K. S. Sim, F. F. Ting, J. W. Leong, and C. P. Tso, "Signal-to-noise ratio estimation for SEM single image using cubic spline interpolation with linear least square regression," *Engineering Letters*, vol. 27, no. 1, pp151-165, 2019.
[20] C. Toa, K. Sim, Z. Lim, and C. Lim, "Magnetic resonance imaging noise filtering using adaptive polynomial-fit non-local means," *Engineering Letters*, vol. 27, no. 3, pp527-540, 2019.
[21] Y. Xu, J. Wen, L. Fei, and Z. Zhang, "Review of Video and Image Defogging Algorithms and Related Studies on Image Restoration and Enhancement," *IEEE Access*, vol. 4, no. 1, pp165-188, 2017.
[22] H. Hu and Y. Guo, "Endoscopic artefact detection in MMDetection," in *EndoCV 2020 Proceedings of the 2nd International Workshop and Challenge on Computer Vision in Endoscopy*, 3 April, 2020, Iowa City, U.S.A., pp78-79.
[23] L. Zabawa, A. Kicherer, L. Klingbeil, R. Toepfer, and R. Roscher, "Counting of grapevine berries in images via semantic segmentation using convolutional neural networks," *ISPRS Journal of Photogrammetry and Remote Sensing*, vol. 164, pp73-83, 2020.